Supporting Information for "Dynamics of equilibrium folding and unfolding transitions of titin immunoglobulin domain under constant forces"

Hu Chen, Guohua Yuan, Ricksen S. Winardhi, Mingxi Yao, Ionel Popa, Julio M. Fernandez, and Jie Yan*

E-mail: phyyj@nus.edu.sg

*To whom correspondence should be addressed

Supporting figures

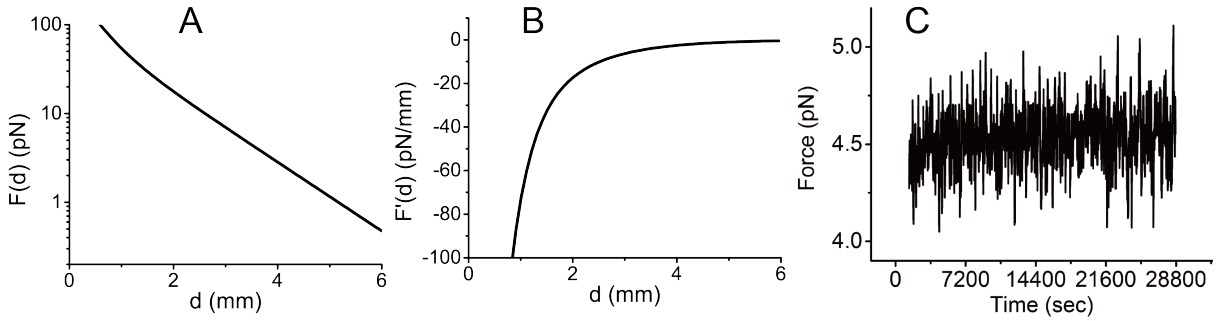

Figure S1: (A) Typical force as a function of the distance between magnets and M270 Dynabead. (B) The sensitivity of force to the distance between magnets and M270 Dynabead is obtained by the derivative of force to distance (Figure A). (C) Time trace of the force measured by bead fluctuation in eight hours at a constant magnets-bead distance using data from the constant force equilibrium measurement in Figure 3A. The force calculated in one-minute sliding time window across the whole time course remains nearly constant at 4.53 ± 0.15 pN, demonstrating that over this eight hours time scale, the force drift is negligible.

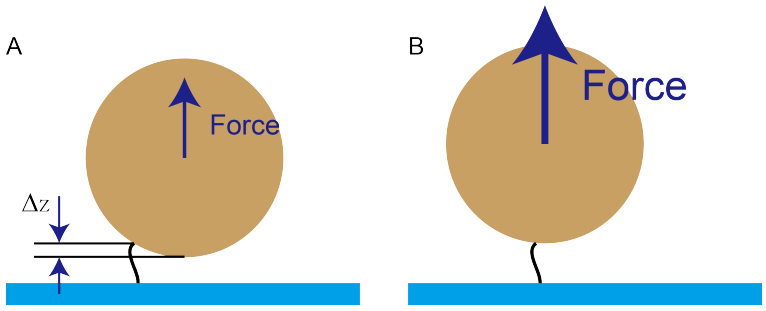

Figure S2: Bead orientation makes the measured extension deviate from the absolute extension of the protein construct. (A) In most cases, the tether point on the bead is not at the bottom pole of the bead. Δz induces uncertainty of extension measurement. (B) When force increases, the orientation of the bead can change and induce change of Δz.

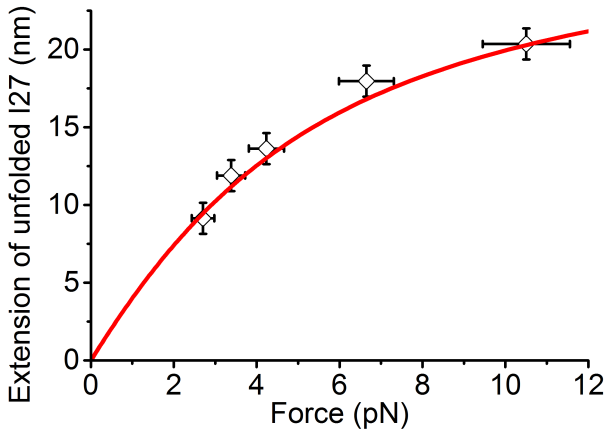

Figure S3: Extension of unfolded I27 as a function of stretching force $x_{\mathrm{chain}}(\mathrm{f})$ measured from a single protein tether. Data points show the measured force-extension curve, and the red curve is the theoretical curve of WLC model with persistence length of 0.8 nm and contour length of 33 nm.

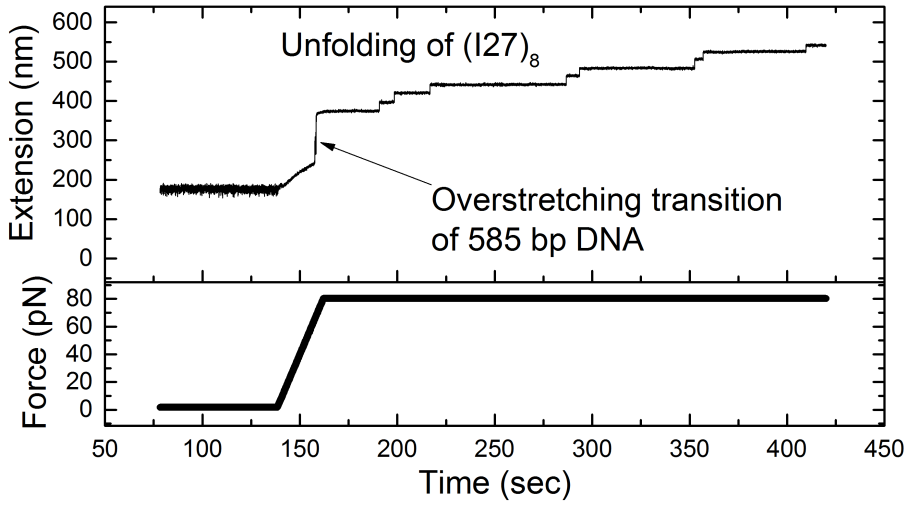

Figure S4: DNA overstretching transition and unfolding of $(\mathrm{I27})_8$. The extension change during force increase to 80 pN with constant loading rate of $\sim$ 3.3 pN/sec shows the DNA overstretching transition at $\sim$ 67 pN with an extension increase of $\sim$ 126 nm, which is consistent with the expected overstretching length of 585 bp DNA.[1–3] Holding the tether at a constant force of 80 pN, eight characteristic unfolding steps of I27 were observed. Besides these specific DNA and I27 signals, no other nonspecific unfolding steps were observed.

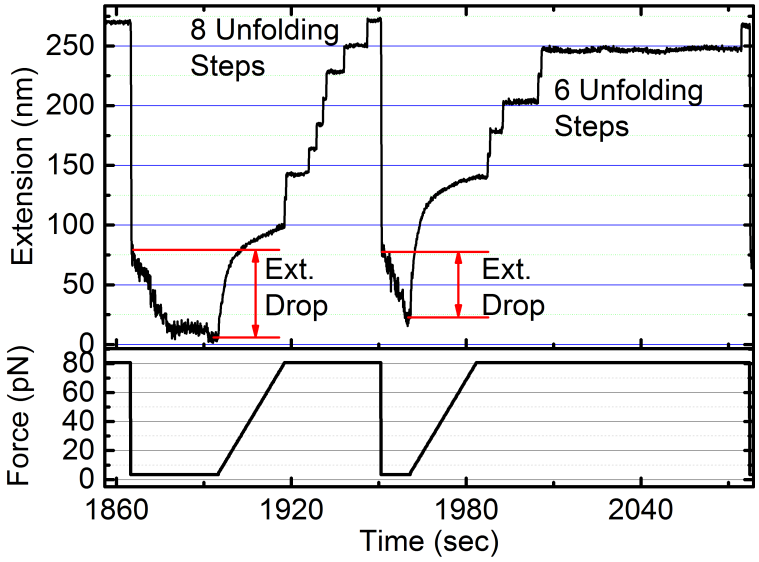

Figure S5: The extension drop under constant force of 3.4 ± 0.4 pN is correlated with the number of folded I27 which is counted by the number of ~~unfolded~~ steps in the following force-increase scan. The extension drop values in Figure 2B and S6 were obtained by this method.

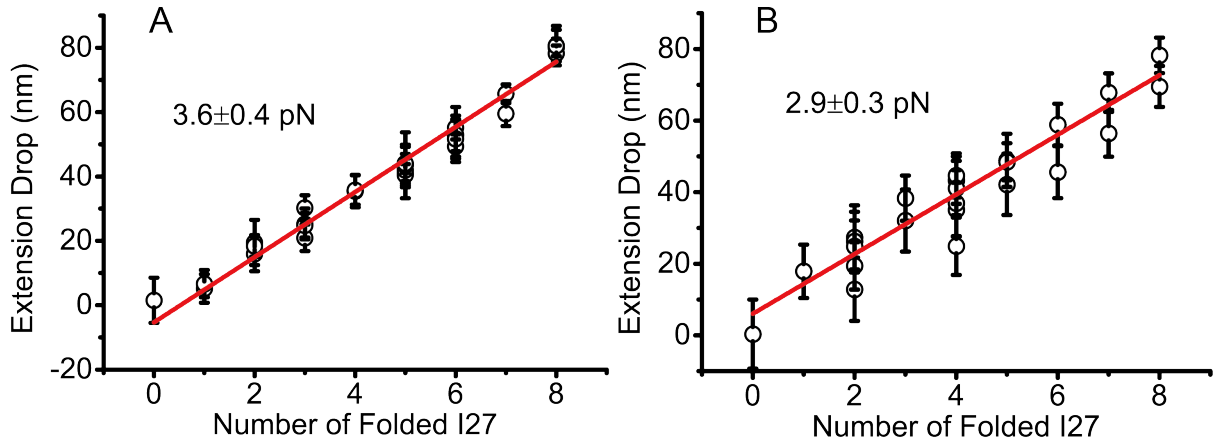

Figure S6: The correlation between the extension drop during the folding process (Figure S5) and the number of successfully folded I27 counted in a following force-increase scan. (A) At force of 3.6 ± 0.4 pN, linear fitting result of the red line gives $R^2 = 0.98$. (B) At force of 2.9 ± 0.3 pN, linear fitting result of the red line gives $R^2 = 0.91$. Error bar is given by the standard deviation of extension fluctuation in 0.3 second time window.

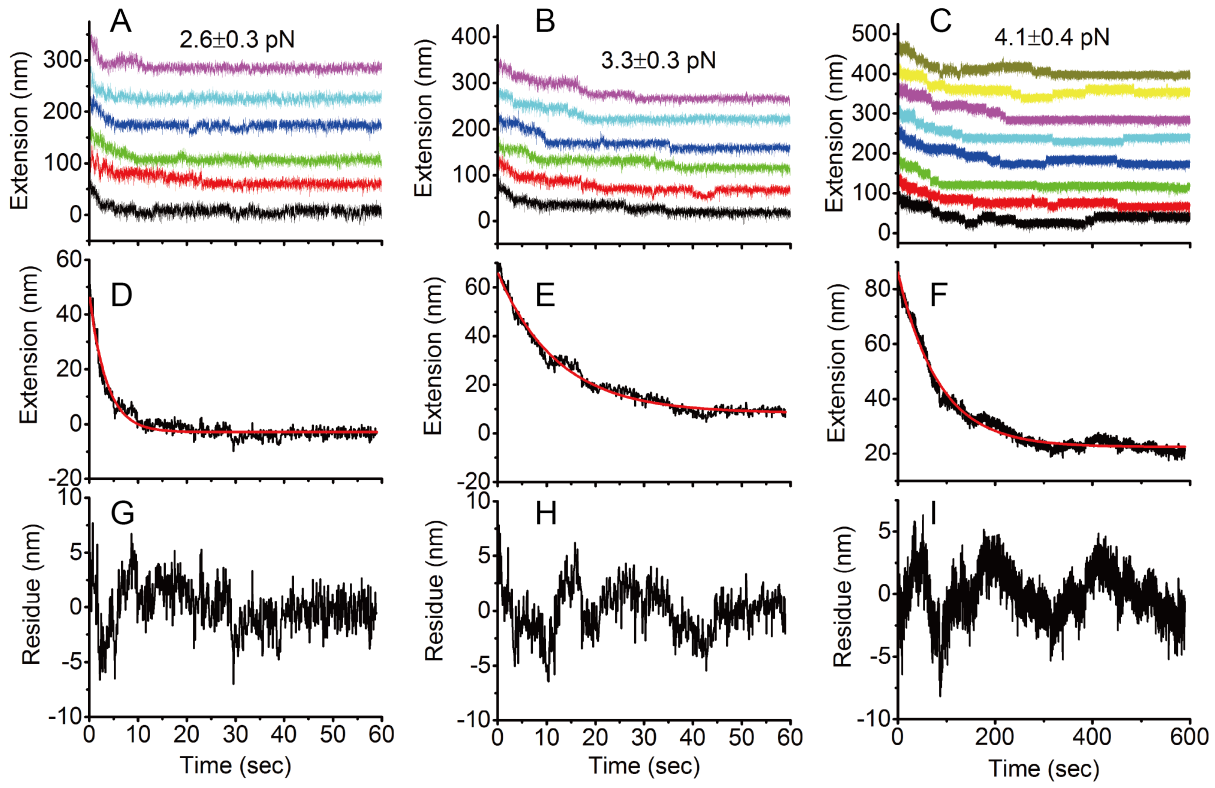

Figure S7: Individual folding time courses and exponential fitting results. (A) Six folding time courses at force of 2.6 ± 0.3 pN. The numbers of correct folded I27 repeats are 8, 7, 8, 8, 8, 7 from top to bottom, respectively, which were counted in following force-increase scans. (B) Six folding time courses at force of 3.3 ± 0.3 pN. The numbers of correct folded I27 repeats are 8, 7, 8, 7, 7, 7 from top to bottom, respectively. (C) Eight folding time courses at force of 4.1 ± 0.4 pN. The numbers of correct folded I27 repeats are 8, 7, 8, 7, 8, 8, 7, 6 from top to bottom, respectively. (D-I) The fitting of exponential extension curves and fitting residues during folding at forces of 2.6 ± 0.3 pN (D,G), 3.3 ± 0.3 pN (E,H), and 4.1 ± 0.4 pN (F,I). The fitting results give R^2 =0.93, 0.98, and 0.98 for 2.6 pN, 3.3 pN, and 4.1 pN, respectively.

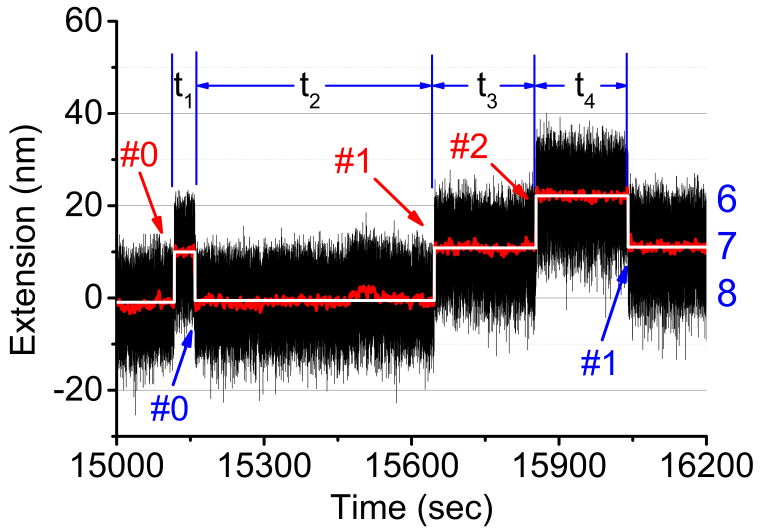

Figure S8: Definition of pseudo unfolding and folding dwell time. The time course in Figure 3A was zoomed in to show several detailed unfolding and folding steps. In this time window of 20 minutes, there are three unfolding events indicated by red arrows and two folding events indicated by blue arrows. The number of folded I27 repeats is given on the right side of the figure. Pseudo unfolding/folding dwell time of each unfolding/folding event is calculated from the time intervals and the number of folded domains between two adjacent unfolding/refolding events. For example, Pseudo unfolding time of #1 unfolding event is $7t_1 + 8t_2$, while pseudo unfolding time of #2 unfolding event is $7t_3$. Pseudo folding time of #1 folding event is $t_3 + 2t_4$. Pseudo unfolding/refolding dwell time corresponds to the unfolding/folding time of one I27 domain.[4]

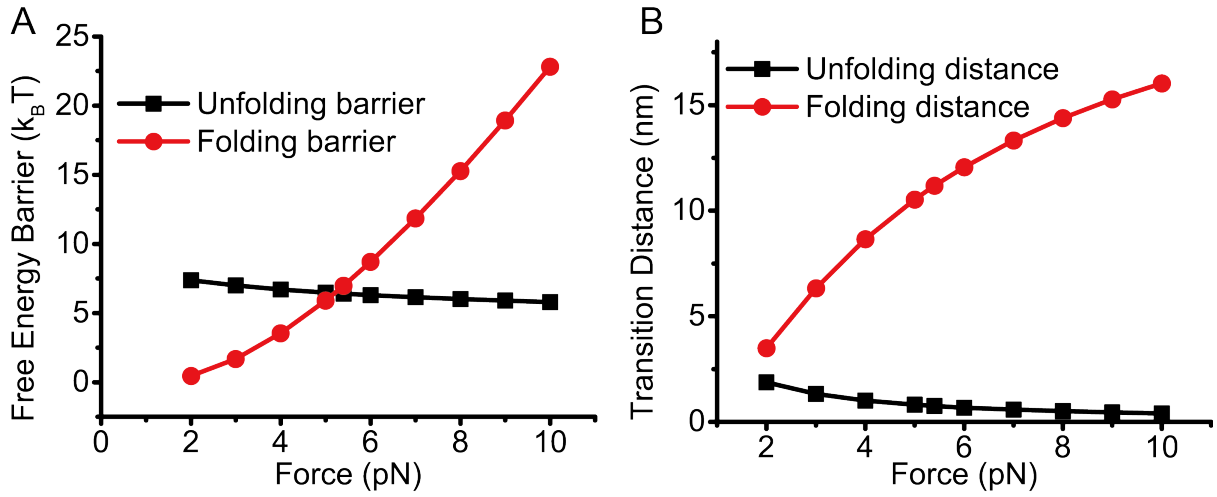

Figure S9: (A) Force-dependent unfolding and folding free energy barriers are calculated from the free energy landscape (Figure 4). Unfolding barrier is much less sensitive to force than folding barrier, expected from the small unfolding transition distance. (B) Force-dependent unfolding and folding transition distances, $\delta_{\text{unfolding}}(F)$ and $\delta_{\text{folding}}(F)$ are calculated from the free energy landscape (Figure 4). The transition state is located at extension of $x_c \sim 4$ nm.

Force stability of magnetic tweezers

Force is a function of the distance between permanent magnets and the paramagnetic beads d, which was calibrated by 16 μm λ DNA as described in our previous publication.[5] For the magnets pair we were using, the force equation is given by

$$f = C * (exp(-d/0.36) + 0.48 * exp(-d/1.12)),$$

where d is in unit of millimeter (mm), and C is a constant which is determined by the properties of paramagnetic bead. For M270 beads we used in experiment, $C \sim 210$ pN. A constant force was achieved by maintaining a constant d. Figures S1A-B show $F(d)$ and its derivative $F'(d)$, respectively. From the $F'(d)$ curve, at the low force range ($F < 10$ pN), the slope is less than 0.01 pN/μm. Such ultra-small stiffness results in excellent force stability against change in d due to thermal drift.

In order to demonstrate the force stability of our magnetic tweezers, Figure S1C shows a long time course of force calculated based on thermal fluctuation of the bead in one-minute sliding time window during which the magnets were not moving using equation

$$f = \frac{k_{\mathrm{B}}T(R+z)}{\delta_y^2}, \tag{S1}$$

where R is the radius of the paramagnetic bead which is set as 1.4 um for typical M270 Dynabead, z is the extension of protein tether, and δ_y^2 is the variance of transverse fluctuation of the paramagnetic bead perpendicular to the magnetization direction. Here the assumption is that the tether point is the bottom pole of the paramagnetic bead. The result indicates that over eight hours the force remained as a constant around 4.5 pN. Due to the high corner frequency of the transverse fluctuation of short tethers like single protein, such force calibration based on thermal fluctuation can only be done for small forces (< 15 pN).[5] At higher forces, force can be obtained by extrapolation using the calibration curve Figure S1A.

Due to the uncertainty of bead size R and the deviation of tether point from the bottom pole of the bead, the calibrated force has $\sim 10\%$ uncertainty.

Extension and stepsize measurement

In the magnetic tweezers measurements, the extension of the tether is indicated by the height of the bead from the surface and measured based the calibrated bead diffraction pattern.[6,7] Theoretically, the extension of the molecule can be obtained by adding an offset Δ based on the known contour length of molecule at high force. However, it has been well known that ~~the~~ each bead has a preferred magnetization direction,[8] forcing the bead to rotate to align the preferred magnetization axis with the magnetic field that is perpendicular to the force direction in our magnetic tweezers (Fig. S2). As a result, in most cases, the tethering point between the molecule and the bead is off-center, and the off-aligned tension in the tether f and the force on the bead F applied by the magnets leads to a torque, which is balanced by the torque from the tendency of aligning the preferred magnetization axis along the magnetic field (Figure S2).

Together, the orientation of the bead is determined by both force balance and torque balance, which contributes to the actual height of bead in addition to the extension of the tether. Force change causes torque change and therefore reorientation of the bead. The offset Δ between the bead height and the tether extension therefore depends on force and cannot be treated as a constant. As a result, the extensions of short tethers that require nm accuracy cannot be directly measured. What can be measured is the extension change at constant forces, such as protein unfolding and refolding steps $\Delta x(f)$, at which the torque remains balanced.

In a protein unfolding problem, the force-extension curve $x_{\text{chain}}(f)$ of the unfolded peptide chain can be obtained from $\Delta x(f)$ if the the force-extension curve of the folded protein is known by the following equation: $x_{\text{chain}}(f) = \Delta x(f) + x_{\text{folded}}(f)$. Figure S3 shows the

force-extension curve of the unfolded I27 peptide chain using this method.

Force-extension curves

The force-extension curve of unfolded I27 polypeptide can be modeled as a worm-like chain (WLC) polymer and described by the Marko-Siggia formula:[9]

$$\frac{fA}{k_{\mathrm{B}}T} = \frac{1}{4(1 - x_{\mathrm{chain}}/L)^2} - \frac{1}{4} + \frac{x_{\mathrm{chain}}}{L}, \tag{S2}$$

where f is force, A is the persistence length, k_{B} is the Boltzmann constant, T is the absolute temperature, x_{chain} is the extension along force direction, and L is the contour length of the polymer. At low force region, unfolded I27 has persistence length of $A \sim 0.8$ nm,[10] and contour length of $L \sim 33$ nm.[11]

At low force, the folded I27 can be modeled as a rigid rod with size of $l_0 = 4$ nm. When a force f is applied to the N-terminus and C-terminus of an I27 monomer, the orientational energy of the protein is given by

$$E(\hat{t}) = -f\hat{x} \cdot l_0\hat{t},$$

where unit vector $\hat{x}$ is the force direction, and unit vector $\hat{t}$ is the orientation of the vector connecting the N- and C- termini. Therefore, in spherical coordinate choosing force direction as the zenith direction, the partition function is given by:

$$Z = \int_0^{2\pi} d\phi \int_0^{\pi} \exp(-E(\hat{t})/k_{\mathrm{B}}T)\sin(\theta)d\theta = 4\pi\frac{\sinh(fl_0/k_{\mathrm{B}}T)}{fl_0/k_{\mathrm{B}}T}.$$

The average extension of I27 along force direction can be obtained by:

$$x = k_{\mathrm{B}}T\frac{\partial \ln Z}{\partial f},$$

which gives force extension curve of folded I27:

$$\frac{x_{\mathrm{I27}}}{l_0} = \coth \frac{f l_0}{k_{\mathrm{B}} T} - \frac{k_{\mathrm{B}} T}{f l_0}. \tag{S3}$$

This form is identical to the monomeric force-extension curve in the freely-joint chain (FJC) polymer model, because each monomer in FJC is a rigid rod.

Extension difference of unfolded polypeptide chain and folded I27 is denoted as $\Delta x(f) = x_{\mathrm{chain}}(f) - x_{\mathrm{I27}}(f)$, where $x_{\mathrm{chain}}(f)$ is inverse function of Eq.(S2). $\Delta x(f)$ was measured in experiments directly, while the force extension curve of the unfolded I27 peptide was obtained by adding back the theoretical force-extension curve of the folded I27 (Eq. S3): $x_{\mathrm{chain}}(f) = \Delta x(f) + x_{\mathrm{I27}}(f)$, as shown in Figure S3.

Specificity of the surface functionalization and tethering chemistry

In order to demonstrate the specificity of the surface functionalization and tethering chemistry, we stretched a chimeric molecule HaloTag-$(\mathrm{I27})_8$-DNA(585 bp)-biotin tethered between the Halo-ligand coated coverslip surface and streptavidin-coated M270 Dynabead. During force increase from zero to about 80 pN with a constant loading rate of $\sim$ 3.3 pN/sec, the recorded extension change of the construct shows the characteristic DNA overstretching transition at $\sim$ 65 pN indicated by a large extension increase by $\sim$ 67% of the contour length, followed by eight characteristic unfolding steps of I27 units in the $(\mathrm{I27})_8$ construct (Figure S4).

Derivation of the free energy landscape

In a magnetic tweezers experiment, the molecule is subject to an external force constraint of F applied by the pair of magnets to the paramagnetic bead. A tension f is established inside the molecule, and at equilibrium the tension and the external force balance. The

tension depends on the extension of the molecule through the force-extension curve $f(x)$. The conformational free energy at extension x can be defined as: $\phi(x) = \int_0^x f(x')dx'$, which is related to $f(x)$ through the derivative: $f(x) = d\phi(x)/dx$. $\phi(x)$ is a monotonically increasing function since $f(x) > 0$. Under a constraint of an external force F, the extension-dependent conformational free energy becomes: $\phi^F(x) = \phi(x) - Fx$. It has an energy minimum located at $x_{\rm eq}(F)$ determined by $d\phi^F(x_{\rm eq})/dx = 0$, at which the equilibrium is reached and the tension balances the external force: $f(x_{\rm eq}) = F$.[12]

For a molecule that only has a folded rigid body state and an unfolded flexible peptide chain state, one can write the energy of the states as: $G^F_{\rm I27}(x) = \phi^F_{\rm I27}(x) - \Delta G_0$, and $G^F_{\rm chain}(x) = \phi^F_{\rm chain}(x)$, respectively, where ΔG_0 is the folding energy of the folded state at zero force. The larger ΔG_0, the more stable the folded sate.

$G^F_{\rm I27}(x)$ and $G^F_{\rm chain}(x)$ can be calculated based on their respective force-extension curves. Free energy of folded I27 can be calculated as a function of extension along force direction by equation:

$$G^F_{\rm I27}(x) = -\Delta G_0 + \int_0^x f_{\rm I27}(x')dx' - Fx, \tag{S4}$$

where $f_{\rm I27}(x')$ is the inverse function of Eq. (S3). Free energy of unfolded polypeptide chain as a function of extension can be obtained by equation:

$$G^F_{\rm chain}(x) = \int_0^x f_{\rm chain}(x')dx' - Fx, \tag{S5}$$

where $f_{\rm chain}(x')$ is obtained from Eq. (S2).

The partition function of the system as a function of extension is given by

$$Z^F(x) = \exp(-G^F_{\rm I27}(x)/k_{\rm B}T) + \exp(-G^F_{\rm chain}(x)/k_{\rm B}T). \tag{S6}$$

Therefore, the free energy landscape along extension is

$$G^F(x) = -k_{\rm B}T \ln Z^F(x), \tag{S7}$$

which gives Eq.(6) in main text which describes the free energy landscape using the extension as the transition coordinate.

Discussion of the free energy landscape

The free energy landscape described by the extension as the transition coordinate in Eq. (6) is a strict result from statistical mechanics for a two-state transition, with an underlying approximation that the folded state is an ideal rigid body and the unfolded state is a flexible polymer. The meaning and applications of this free energy landscape are explained with details below.

Here we discuss the meanings of the transition state, transition distances and energy barrier in this two-state system. The transition state is located at the peak of the free energy landscape, which is approximately the critical extension $x_{\rm c}$ at which the probabilities of the folded and unfolded states are equal. Therefore, it follows that $G^F_{\rm I27}(x_{\rm c}) = G^F_{\rm chain}(x_{\rm c})$, or $\phi^F_{\rm I27}(x_{\rm c}) - \phi^F_{\rm chain}(x_{\rm c}) = \Delta G_0$. In addition, since $\phi^F_{\rm I27}(x_{\rm c}) - \phi^F_{\rm chain}(x_{\rm c}) = \phi_{\rm I27}(x_{\rm c}) - \phi_{\rm chain}(x_{\rm c})$, the transition state in the two state system has no force dependence. The force-dependent unfolding and refolding transition distances are determined by $\delta_{\rm unfold}(F) = x_{\rm c} - x^{eq}_{\rm I27}(F)$ and $\delta_{\rm fold}(F) = x^{eq}_{\rm I27}(F) - x_{\rm c}$, respectively. Below we discuss the advantages and limitations of applying such a simple two-state free energy landscape to understand real experiments.

An obvious advantage is that, despite its simplicity, it covers several essential aspects that are typically involved in mechanical unfolding and refolding of proteins. Compared with the flexible unfolded state with longer contour length, the small size rigid body of the folded state results in a much steeper increase in $\phi^F_{\rm I27}(x)$ than $\phi^F_{\rm chain}(x)$ as x increases.

As a result, the transition state $x_{\rm c}$ is close to the equilibrium extension of the folded state $x^{eq}_{\rm I27}(F)$. This ensures a small unfolding transition distance $\delta_{\rm unfold}(F)$, which is consistent with the typically observed sub-nanometer unfolding transition distance in force-induced protein unfolding. In addition, as a rigid body of nanometer size l is aligned up by force

$k_{\mathrm{B}}T/l$ in the scale of several pN, at large forces ($F > k_{\mathrm{B}}T/l$) its extension approaches l and therefore $\delta_{\mathrm{unfold}}(F)$ has a weak force-dependence which can be approximated as a constant, approaching zero at high force.

As a result of the insensitive dependence on force, the Bell's model using a constant unfolding transition distance is always a good approximation to describe the force dependent unfolding rate. In contrast, the folding transition distance, $\delta_{\mathrm{fold}}(F) = x^{eq}_{\mathrm{chain}}(F) - x_{\mathrm{c}}$, has a much more prominent force dependence due to the nature of the flexible unfolded polymer chain with a much longer contour length. This is the reason why the Bell's model is no longer a good approximation to describe the force dependent folding rate and one has to calculate $\delta_{\mathrm{fold}}(F)$ based on the force-extension curve of the unfolded chain. For the reasons above, the model predicts a linear force dependence of the unfolding rate on logarithm scale, and a nonlinear force dependence of the refolding rate on logarithm scale, which are observed in our experiment for I27 (Fig. 2E), in previous experiments by Schlierf, et al.,[13] and in our other experiments for G-quadruplex structures (under review).

Here we discuss the limitation of this simple two-state model. Due to the ideal rigid body assumption, the unfolding transition distance approaches zero while in real experiment it is typically a non-zero sub-nanometer number. For I27, previous AFM experiments have reported a value of 0.25 nm.[11] In addition, due to its two-state nature, the transition state has the extension at which the two states roughly have equal probabilities. However, in real experiments, the transition state often corresponds to structural intermediates, which are often involving disruption of a few initial molecular interactions. This results in nonzero unfolding transition distance and changes the actual height of energy barrier as well as the transition rates. However, it does not affect the generic nature of a small force-insensitive unfolding transition distance, a large force-sensitive folding transition distance, a linear force dependence of the unfolding rate on logarithm scale, and a nonlinear force dependence of the refolding rate on logarithm scale. Force-dependent unfolding barrier, folding barrier, unfolding distance $\delta_{\mathrm{unfold}}(F)$, and folding distance $\delta_{\mathrm{fold}}(F)$ from the simplified two-state free

energy landscape are shown in Figure S9.

References

(1) Fu, H.; Chen, H.; Zhang, X.; Qu, Y.; Marko, J. F.; Yan, J. *Nucleic Acids Res.* **2011**, *39*, 3473–3481.

(2) Bosaeus, N.; El-Sagheer, A. H.; Brown, T.; Smith, S. B.; Akerman, B.; Bustamante, C.; Norden, B. *Proc. Natl. Acad. Sci. U.S.A.* **2012**, *109*, 15179–15184.

(3) Zhang, X.; Chen, H.; Le, S.; Rouzina, I.; Doyle, P. S.; Yan, J. *Proc. Natl. Acad. Sci. U.S.A.* **2013**, *110*, 3865–3870.

(4) Cao, Y.; Kuske, R.; Li, H. *Biophys. J.* **2008**, *95*, 782–788.

(5) Chen, H.; Fu, H.; Zhu, X.; Cong, P.; Nakamura, F.; Yan, J. *Biophys. J.* **2011**, *100*, 517–523.

(6) Strick, T. R.; Allemand, J. F.; Bensimon, D.; Bensimon, A.; Croquette, V. *Science* **1996**, *271*, 1835–1837.

(7) Gosse, C.; Croquette, V. *Biophys. J.* **2002**, *82*, 3314–3329.

(8) Lipfert, J.; Kerssemakers, J. W.; Jager, T.; Dekker, N. H. *Nat. Methods* **2010**, *7*, 977–980.

(9) Marko, J.; Siggia, E. *Macromolecules* **1995**, *28*, 8759–8770.

(10) Rief, M.; Pascual, J.; Saraste, M.; Gaub, H. *J. Mol. Biol.* **1999**, *286*, 553–561.

(11) Carrion-Vazquez, M.; Oberhauser, A.; Fowler, S.; Marszalek, P.; Broedel, S.; Clarke, J.; Fernandez, J. *Proc. Natl. Acad. Sci. U. S. A.* **1999**, *96*, 3694–3699.

(12) Rouzina, I.; Bloomfield, V. A. *Biophys. J.* **2001**, *80*, 882–893.

(13) Schlierf, M.; Berkemeier, F.; Rief, M. *Biophys. J.* **2007**, *93*, 3989–3998.